

A Relaxed Wasserstein Distance Formulation for Mixtures of Radially Contoured Distributions*

Keyu Chen[†], Zetian Wang[†], and Yunxin Zhang[‡]

Abstract. Recently, a Wasserstein-type distance for Gaussian mixture models has been proposed. However, that framework can only be generalized to identifiable mixtures of general elliptically contoured distributions whose components come from the same family and satisfy marginal consistency. In this paper, we propose a simple relaxed Wasserstein distance for identifiable mixtures of radially contoured distributions whose components can come from different families. We show some properties of this distance and that its definition does not require marginal consistency. We apply this distance in color transfer tasks and compare its performance with the Wasserstein-type distance for Gaussian mixture models in an experiment. The error of our method is more stable and the color distribution of our output image is more desirable.

Key words. optimal transport, Wasserstein distance, mixture models, radial basis functions, barycenter, image processing application

MSC codes. 49Q22, 62H30, 65K05, 65K10, 68U10, 65D12

1. Introduction. In recent years, optimal transport (OT) has attracted a lot of attention in mathematics [14], engineering [28], data science [23] and imaging science [3, 22]. This work was originally considered by Monge [27] and has significantly developed after Kantorovich's work [21]. The main purpose of optimal transport is to measure the distance of two probability distributions, known as Wasserstein distance, and to find an optimal transport map between the two distributions. In practice, optimal transport is formulated with a linear programming problem. As an aspect of applied mathematics, the computation method plays an important part in OT-related work. The basic solvers of OT are the classic linear programming solvers such as simplex method and inner point method [7]. They have a complexity of $O(n^3)$, and thus the computation is expensive in large-scale problems. Recently, some fast algorithms have been proposed, enabling OT to deal with such problems, such as Sinkhorn algorithm [9], Greenkhorn algorithm [2], and others [17, 13, 25].

Another way to reduce the computation is trying to reduce the amount of data. A natural way is that we can sample part of data, compute the Wasserstein distance several times and take the average value. Alternatively, one may use the expectation of Wasserstein distance between empirical distributions to approximate the true Wasserstein distance. This method was first researched in [12], which proved that the expectation of the Wasserstein distance between empirical distributions converge in expectation to the true Wasserstein distance and

*Submitted to the editors DATE.

Funding: This research is supported by National Key R&D Program of China (2024YFA1012401), the Science and Technology Commission of Shanghai Municipality (23JC1400501), and Natural Science Foundation of China (12241103).

[†]School of Mathematical Sciences, Fudan University, Shanghai 200433, China. (chenky21@m.fudan.edu.cn, wangzt24@m.fudan.edu.cn).

[‡]Shanghai Key Laboratory for Contemporary Applied Mathematics, Laboratory of Mathematics for Nonlinear Science, Fudan University, Shanghai 200433, China. (xyz@fudan.edu.cn).

gave a convergence rate. More careful discussion about the convergence behavior can be found in [5, 4, 31].

However, in practice, we usually not only need the Wasserstein distance but also need to find a map that transports one distribution to another. For instance, while dealing with color transfer task, what we actually need is only the transfer map. The sample-based method can not handle this task. Another way to reduce complexity is to add some structure to the data, which is easier to operate than discrete distributions. The Gaussian mixture models (GMMs) comes first. It is a popular probability model in statistics and machine learning [19]. Thanks to the EM algorithm [11], the parameters of GMMs are easily inferred. In image processing, it is used in a large body of works to represent the patch distributions of images, such as image restoration [35, 33, 30] and texture synthesis [15]. Recently, a Wasserstein-type distance in the space of GMMs has been proposed in [10]. Based on the explicit formulation of the Wasserstein distance and optimal transport map for Gaussian distributions, they give two ways to define a transport map. Their method is shown useful in color transfer task and texture synthesis task.

The work based on GMMs relies on that GMMs can approximate distributions well. If we view it as a function approximation problem, it is approximating a function with Gaussian basis weighted by normalized positive coefficients. However, Gaussian density function is elliptically contoured, which includes a positive definite matrix as parameters. In function approximation field, radial basis function (RBF) is widely used as basis. It performs well in unary and multivariate function approximation [24, 32, 34]. Compared to Gaussian density function, the number of parameters, instead of a positive definite matrix, reduces to only 1. Thus when faced with high-dimensional problems, approximation using RBFs requires much fewer parameters than Gaussian density functions. Moreover, the method based on GMMs requires approximating both the two distributions with GMMs. However, using the basis functions in the same family to approximate two functions would not be reasonable in many situations. We may need to use two different families of basis functions to approximate the two functions. [8] gives the optimal transport map and Wasserstein distance between distributions with radial density functions, which we call radially contoured distributions, and shows that the Wasserstein barycenter of such distributions is still radial. Thus we can establish a framework for finite mixtures of radially contoured distributions, which we call radial mixture models (RMMs).

In this paper, we focus on the space W_2 . Instead of restricting the possible coupling measures to GMMs in [10], we view RMMs as discrete distributions in the space of radially contoured distributions and define a distance for RMMs as the Wasserstein distance of their corresponding discrete distributions. We prove the parallel version for RMMs of important theorems for GMMs. Rather than requiring the components of identifiable mixtures of elliptically contoured distributions to be all of one type and satisfy marginal consistency in [10], RMMs consist of components that can come from different families and do not need to satisfy marginal consistency. To infer the parameters of RMMs in application, we introduce the mini-batch stochastic technique to speed up the EM algorithm for RMMs. At last of this paper, we provide an application to color transfer task and compare our method with that proposed in [10] based on GMMs. The result shows that our method is more numerically stable and the transferred color distribution is more reasonable.

The paper is organized as follows. In section 2, we recall the related results about Wasserstein distance and barycenter, especially for radially contoured distributions, and the Wasserstein-type distance GW_2 for GMMs proposed in [10]. In section 3, we define RW_2 distance for identifiable finite mixtures of radially contoured distributions and prove a parallel version of the important properties of GMMs. We discuss in subsection 3.6 that we can remove the marginal consistency that is important in [10]. In section 4, we conduct some toy experiments to show the difference between RW_2 and W_2 . In section 5, we show how to apply our method in practice. We compare our method with GW_2 in a color transfer task, and find that our method is more desirable in this experiment. Finally, we conclude our work in section 6 and provide some ways to which this work can be extended in the future.

2. Review of related results.

2.1. Wasserstein distance and barycenter. Let $d \geq 1$ be an integer. We write $\mathcal{P}(\mathbb{R}^d)$ the set of probability measures on \mathbb{R}^d . For $p \geq 1$, the Wasserstein space $\mathcal{P}_p(\mathbb{R}^d)$ is defined as the set of probability measures with finite moment of order p , that is,

$$\mathcal{P}_p(\mathbb{R}^d) = \left\{ \mu \in \mathcal{P}(\mathbb{R}^d) : \int_{\mathbb{R}^d} \|x\|^p d\mu(x) < +\infty \right\}.$$

From now on, we will focus on the case $p = 2$.

Given $\mu_0, \mu_1 \in \mathcal{P}_2(\mathbb{R}^d)$, a transport map T from μ_0 to μ_1 is a measure preserving map, i.e. for every measurable set $A \subset \mathbb{R}^d$, $\mu_0(T^{-1}(A)) = \mu_1(A)$. The Monge formulation of optimal transport is

$$(2.1) \quad \inf_{T: T_{\#}\mu_0 = \mu_1} \int_{\mathbb{R}^d} \|x - T(x)\|^2 d\mu_0(x),$$

where $T : T_{\#}\mu_0 = \mu_1$ means that T takes over all measurable transport maps from μ_0 to μ_1 . The optimal T is called Monge map transporting μ_0 to μ_1 . Define $\Pi(\mu_0, \mu_1) \subset \mathcal{P}_2(\mathbb{R}^d \times \mathbb{R}^d)$ as the subset of probability distributions γ on $\mathbb{R}^d \times \mathbb{R}^d$ with marginals μ_0 and μ_1 . Specifically, $(P_0)_{\#}\gamma = \mu_0$ and $(P_1)_{\#}\gamma = \mu_1$, where P_0 and P_1 are natural projections from $\mathbb{R}^d \times \mathbb{R}^d$ to \mathbb{R}^d . Kantorovich gives a relaxed form of (2.1) by

$$(2.2) \quad W_2(\mu_0, \mu_1)^2 = \inf_{\gamma \in \Pi(\mu_0, \mu_1)} \int_{\mathbb{R}^d \times \mathbb{R}^d} \|x - y\|^2 d\gamma(x, y).$$

$W_2(\cdot, \cdot)$ actually defines a distance on $\mathcal{P}_2(\mathbb{R}^d)$, which is known as the Wasserstein distance.

If T is a Monge map transporting μ_0 to μ_1 , the path $(\mu_t)_{t \in [0,1]}$ given by

$$(2.3) \quad \mu_t = (T_t)_{\#}\mu_0, \quad T_t(x) = (1-t)x + tT(x), \quad \forall t \in [0, 1]$$

defines a constant speed geodesic curve on $(\mathcal{P}_2(\mathbb{R}^d), W_2)$, i.e.

$$(2.4) \quad W_2(\mu_s, \mu_t) = (t-s)W_2(\mu_0, \mu_1), \quad 0 \leq s \leq t \leq 1.$$

This path is called McCann interpolation [26] between μ_0 and μ_1 . It satisfies

$$(2.5) \quad \mu_t \in \arg \min_{\mu \in \mathcal{P}_2(\mathbb{R}^d)} (1-t)W_2(\mu_0, \mu)^2 + tW_2(\mu_1, \mu)^2.$$

The McCann interpolation can be generalized to more than two distributions, which is known as Wasserstein barycenter. Given an integer $N \geq 2$, N probability measures $\mu_1, \mu_2, \dots, \mu_N$ and weights $\lambda = (\lambda_1, \lambda_2, \dots, \lambda_N) \in \Gamma_N$, where Γ_N is the N -probability simplex, the associated Wasserstein barycenter problem is

$$(2.6) \quad BW_2(\mu_1, \mu_2, \dots, \mu_N)^2 = \inf_{\mu \in \mathcal{P}_2(\mathbb{R}^d)} \sum_{j=1}^N \lambda_j W_2(\mu_j, \mu)^2.$$

A solution of the previous problem is called the Wasserstein barycenter of probability measures $\{\mu_j\}_{j=1}^N$ with weights $\{\lambda_j\}_{j=1}^N$. The existence and uniqueness have been deeply studied in [1].

2.2. Results for radially contoured distributions. The results in this section can be found in [8]. A d -dimensional radially contoured distribution μ on \mathbb{R}^d is a probability measure and

$$d\mu(x) = \frac{1}{Z} \rho \left(\frac{\|x - m\|}{c} \right) dx,$$

where ρ is a nonnegative measurable function or Dirac- δ function on \mathbb{R}_+ and Z is the normalizer that ensures $\int_{\mathbb{R}^d} d\mu(x) = 1$. In this paper, we mainly focus on the case that ρ is continuous. For simplicity, we write $\rho(x; m, c)$ for $\rho(\|x - m\|/c)$. We call ρ the generator of μ . We denote $\mu = R_d(m, c, \rho)$. If $c = 1$, we simply denote $\mu = R_d(m, \rho)$. Moreover, we will assume $\mu \in \mathcal{P}_2(\mathbb{R}^d)$. By straightforward calculation, we can get the normalizer, expectation and covariance of a radially contoured distributions as follows: let $X \sim \mu = R_d(m, c, \rho) \in \mathcal{P}_2(\mathbb{R}^d)$, then

$$Z = c^d |\mathbb{S}^{d-1}| \int_0^{+\infty} r^{d-1} \rho(r) dr, \quad E[X] = m, \quad \text{Cov}[X] = \frac{c^2}{d} \frac{\int_0^{+\infty} r^{d+1} \rho(r) dr}{\int_0^{+\infty} r^{d-1} \rho(r) dr} I_d,$$

where $|\mathbb{S}^{d-1}| = 2\pi^{d/2}/\Gamma(d/2)$ denotes the volume of \mathbb{S}^{d-1} .

Let $\mu_0 = R_d(m_0, \rho_0)$, $\mu_1 = R_d(m_1, \rho_1)$ be two radially contoured distributions on \mathbb{R}^d . Considering two 1-dimensional radially contoured distributions $\tilde{\mu}_0 = R_1(0, r^{d-1}\rho_0(r))$ and $\tilde{\mu}_1 = R_1(0, r^{d-1}\rho_1(r))$, and the Monge map C transporting $\tilde{\mu}_0$ to $\tilde{\mu}_1$, then the Monge map T transporting μ_0 to μ_1 is given by

$$(2.7) \quad T(x) = \frac{C(\|x - m_0\|)}{\|x - m_0\|} (x - m_0) + m_1.$$

The McCann interpolation is given by $\mu_t = R_d(m_t, \rho_t)$, where $m_t = (1-t)m_0 + tm_1$ and ρ_t satisfies

$$(2.8) \quad \rho_t(C_t(r)) C_t(r)^{d-1} dC_t(r) = \rho_0(r) r^{d-1} dr,$$

where $C_t(r) = (1-t)r + tC(r)$. The Wasserstein distance is given by

$$W_2(\mu_0, \mu_1)^2 = \|m_0 - m_1\|^2 + |\mathbb{S}^{d-1}| \int_0^{+\infty} (C(r) - r)^2 \rho_0(r) r^{d-1} dr.$$

For $N \geq 2$, it has been proved in [8] that the Wasserstein barycenter μ of radially contoured distributions $\{\mu_j = R_d(m_j, c_j, \rho_j)\}_{j=1}^N$ is still a radially contoured distribution centered at $m_* = \sum_{j=1}^N \lambda_j m_j$.

When the generators of radially contoured distributions are the same, the conclusions above have a simple form. Let $\mu_0 = R_d(m_0, c_0, \rho)$, $\mu_1 = R_d(m_1, c_1, \rho)$, then the Monge map from μ_0 to μ_1 is

$$T(x) = \frac{c_1}{c_0}(x - m_0) + m_1.$$

The displacement interpolation is $\mu_t = R_d(m_t, c_t, \rho)$, where $c_t = (1-t)m_0 + tm_1$, and

$$W_2(\mu_0, \mu_1)^2 = \|m_0 - m_1\|^2 + (c_0 - c_1)^2 \frac{\int_0^{+\infty} r^{d+1} \rho(r) dr}{\int_0^{+\infty} r^{d-1} \rho(r) dr}.$$

For $N \geq 2$, let $\mu_j = R_d(m_j, c_j, \rho_j)$, $j = 1, 2, \dots, N$, and $\lambda = (\lambda_1, \lambda_2, \dots, \lambda_N)$ be the weights. There exists ρ such that barycenter of $\{\mu_j\}_{j=1}^N$ with weights $\{\lambda_j\}_{j=1}^N$ is $\mu = R_d(m_*, c_*, \rho)$, where

$$m_* = \sum_{j=1}^N \lambda_j m_j, \quad c_* = \sum_{j=1}^N \lambda_j c_j.$$

When $\rho_1 = \rho_2 = \dots = \rho_N$, the barycenter is simply $R_d(m_*, c_*, \rho_1)$.

2.3. Wasserstein-type distance for GMM. Let $g_{m, \Sigma}$ be the density function of Gaussian distribution with mean m and covariance Σ . A Gaussian mixture model (GMM) of K components is a probability distribution with density $\rho(x) = \sum_{i=1}^K \pi_i g_{m_i, \Sigma_i}(x)$, where $\pi = (\pi_1, \pi_2, \dots, \pi_K)$ is a weight vector. Let $\mu_0 = \sum_{k=1}^{K_0} \pi_0^k \nu_0^k$ and $\mu_1 = \sum_{l=1}^{K_1} \pi_1^l \nu_1^l$ be two d -dimensional GMMs. In [10], the authors have proposed a Wasserstein-type distance MW_2 , which is formulated as

$$(2.9) \quad MW_2(\mu_0, \mu_1)^2 = \inf_{\gamma \in \Pi(\mu_0, \mu_1) \cap GMM_{2d}(\infty)} \int_{\mathbb{R}^d \times \mathbb{R}^d} \|x - y\|^2 d\gamma(x, y),$$

where μ_0, μ_1 are d -dimensional Gaussian mixture models and $GMM_d(\infty)$ denotes the set of finite mixtures of d -dimensional Gaussian distributions. They show that (2.9) has an equivalent discrete formulation: we can view a GMM as a discrete measure in the space of Gaussian distributions and compute the discrete optimal transport, i.e.

$$(2.10) \quad MW_2(\mu_0, \mu_1)^2 = \inf_{w \in \Pi(\pi_0, \pi_1)} \sum_{k,l=1}^{K_0, K_1} w_{kl} W_2(\nu_0^k, \nu_1^l)^2.$$

MW_2 actually defines a metric on $GMM_d(\infty)$, and $GMM_d(\infty)$ equipped with MW_2 is a geodesic space. The natural MW_2 barycenter problem is

$$(2.11) \quad \inf_{\mu \in GMM_d(\infty)} \sum_{j=1}^N \lambda_j MW_2(\mu_j, \mu)^2,$$

and the solution of (2.11) is called the MW_2 barycenter for N GMMs $\{\mu_j\}_{j=1}^N$, where $\mu_j = \sum_{k=1}^{K_j} \pi_j^{k_j} \nu_j^k$, with weights $\{\lambda_1, \lambda_2, \dots, \lambda_N\}$. They give a discrete formulation of (2.11) which can be computed via linear programming:

$$\inf_{\mu \in \text{GMM}_d(\infty)} \sum_{j=1}^N \lambda_j MW_2(\mu_j, \mu)^2 = \min_{w \in \Pi(\pi_1, \pi_2, \dots, \pi_N)} \sum_{k_1, \dots, k_N=1}^{K_1, \dots, K_N} w_{k_1 \dots k_N} BW_2(\nu_1^{k_1}, \dots, \nu_N^{k_N})^2.$$

They also consider about how to define a map via MW_2 . Let γ^* and w^* be the optimal solutions of (2.9) and (2.10), and $T_{k,l}$ be the Monge map transporting ν_0^k to ν_1^l . Define a discrete probability distribution $\{p_{k,l}(x)\}$ as

$$(2.12) \quad p_{k,l}(x) = \frac{w_{k,l}^* g_{m_0^k, \Sigma_0^k}(x)}{\sum_j \pi_0^j g_{m_0^j, \Sigma_0^j}(x)}.$$

They construct two kinds of maps. The first one is T_{mean} :

$$T_{\text{mean}}(x) = \sum_{k,l=1}^{K_0, K_1} p_{k,l}(x) T_{k,l}(x),$$

and the second one is T_{rand} :

$$T_{\text{rand}}(x) = T_{k,l}(x) \quad \text{with probability } p_{k,l}(x).$$

Compared to T_{mean} , T_{rand} is more mathematically reasonable. They show that for every measurable set A of \mathbb{R}^d ,

$$\int_{\mathbb{R}^d} P(T_{\text{rand}}(x) \in A) d\mu_0(x) = \mu_1(A).$$

It means that $(T_{\text{rand}})_{\#} \mu_0$ is equal to μ_1 in expectation. But in practice, T_{rand} gives a noisier result than T_{mean} . In [10], T_{mean} is used in most of the experiments.

3. The space of radial mixture models equipped with RW_2 distance.

3.1. The definition of radial mixture models and RW_2 distance.

Definition 3.1. Let $K \geq 1$ be an integer. A finite radial mixture μ of size K on \mathbb{R}^d is an identifiable probability measure that can be written as

$$d\mu(x; m, c, \rho) = \sum_{k=1}^K \pi^k d\nu^k(x; m^k, c^k, \rho^k),$$

where $\nu^k = R_d(m^k, c^k, \rho)$, $\pi \in \Gamma_K$, and ρ is a Dirac δ function or nonnegative continuous function which ensures $\mu \in \mathcal{P}_2(\mathbb{R}^d)$. Henceforth, in certain situations, parameters m, c and ρ of μ or ν can be omitted. We also call ρ the generator of radial mixture μ . We denote the set of all radial mixtures generated from ρ on \mathbb{R}^d as $RMM_d(\rho)$ and

$$RMM_d = \cup_{\rho} RMM_d(\rho).$$

Here ρ takes over all functions that promise $RMM_d(\rho)$ is identifiable, i.e. given two mixtures μ_0 and μ_1 in $RMM_d(\rho)$, where

$$d\mu_j(x) = \sum_{k=1}^{K_j} \pi_j^k d\nu_j^k(x), \quad \nu_j^k = R_d(m_j^k, c_j^k, \rho), \quad j = 0, 1,$$

and $\nu_j^k \neq \nu_j^l$ for all $1 \leq k < l \leq K_j$, then $\mu_0 = \mu_1$ if and only if $K_0 = K_1$ and there exists a K_0 -permutation σ such that $\pi_0^{\sigma(k)} = \pi_1^k$ and $\nu_0^{\sigma(k)} = \nu_1^k$ for all $1 \leq k \leq K_0$.

There exist many choices of such ρ . We can view radially contoured distributions as a degeneration of elliptically contoured distributions. The identifiability of finite mixtures of elliptically contoured distributions has been discussed in [20]. For instance, finite mixtures of multi-variate t-distributions are identifiable. The following proposition allows us to approximate distributions in $\mathcal{P}_2(\mathbb{R}^d)$ with radial mixtures.

Proposition 3.2. *$RMM_d(\rho)$ is dense in $\mathcal{P}_2(\mathbb{R}^d)$ with the distance W_2 .*

The proof is similar to that of Proposition 1 in [10]. By viewing radial mixtures as discrete distributions on the space of radially contoured distributions, we deduce a distance for radial mixtures. This distance is analogous to the Wasserstein distance for discrete distributions on Euclidean space.

Theorem 3.3. *Let $\mu_0, \mu_1 \in RMM_d$, where*

$$(3.1) \quad d\mu_j(x) = \sum_{k=1}^{K_j} \pi_j^k d\nu_j^k(x), \quad \nu_j^k = R_d(m_j^k, c_j^k, \rho_j), \quad j = 0, 1,$$

and w^* is a solution of

$$(3.2) \quad \min_{w \in \Pi(\pi_0, \pi_1)} \sum_{k,l=1}^{K_0, K_1} w_{kl} W_2(\nu_0^k, \nu_1^l)^2,$$

then

$$RW_2(\mu_0, \mu_1) = \sqrt{\sum_{k,l=1}^{K_0, K_1} w_{kl}^* W_2(\nu_0^k, \nu_1^l)^2}$$

is a distance on RMM_d . We call $w \in \Pi(\pi_0, \pi_1)$ the RW_2 plan between mixtures μ_0 and μ_1 and w^* the RW_2 optimal plan.

Proof. Apparently, $RW_2(\mu_0, \mu_1) = RW_2(\mu_1, \mu_0)$. For the positive definite property, we will prove $\mu_0 = \mu_1$ if $RW_2(\mu_0, \mu_1) = 0$. Let T_{kl} be the Monge map from ν_0^k to ν_1^l . We define

$$(3.3) \quad d\gamma(x, y) = \sum_{k,l} w_{kl}^* \delta(y - T_{kl}(x)) d\nu_0^k(x) dy,$$

then for all $h \in C(\mathbb{R}^d)$, we have

$$\begin{aligned}
& \int_{\mathbb{R}^d \times \mathbb{R}^d} h(x) d(P_0)_{\#} \gamma(x, y) = \sum_{k,l} \int_{\mathbb{R}^d \times \mathbb{R}^d} h(x) w_{kl}^* \delta(y - T_{kl}(x)) d\nu_0^k(x) dy \\
& = \sum_{k,l} \int_{\mathbb{R}^d} h(x) w_{kl}^* d\nu_0^k(x) = \sum_k \int_{\mathbb{R}^d} h(x) \pi_0^k d\nu_0^k(x) = \int_{\mathbb{R}^d} h(x) d\mu_0(x), \\
& \int_{\mathbb{R}^d \times \mathbb{R}^d} h(y) d(P_1)_{\#} \gamma(x, y) = \sum_{k,l} \int_{\mathbb{R}^d \times \mathbb{R}^d} h(y) w_{kl}^* \delta(y - T_{kl}(x)) d\nu_0^k(x) dy \\
& = \sum_{k,l} \int_{\mathbb{R}^d} h(y) w_{kl}^* d\nu_1^l(y) = \sum_l \int_{\mathbb{R}^d} h(y) \pi_1^l d\nu_1^l(y) = \int_{\mathbb{R}^d} h(y) d\mu_1(y).
\end{aligned}$$

Therefore, $\gamma \in \Pi(\mu_0, \mu_1)$. Moreover,

$$\begin{aligned}
& \int_{\mathbb{R}^d \times \mathbb{R}^d} \|x - y\|^2 d\gamma(x, y) = \sum_{k,l} w_{kl}^* \int_{\mathbb{R}^d \times \mathbb{R}^d} \|x - y\|^2 \delta(y - T_{kl}(x)) d\nu_0^k(x) dy \\
& = \sum_{k,l} w_{kl}^* \int_{\mathbb{R}^d} \|x - T_{kl}(x)\|^2 d\nu_0^k(x) = \sum_{k,l} w_{kl}^* W_2(\nu_0^k, \nu_1^l)^2 = RW_2(\mu_0, \mu_1)^2.
\end{aligned}$$

It follows that

$$W_2(\mu_0, \mu_1)^2 \leq \int_{\mathbb{R}^d \times \mathbb{R}^d} \|x - y\|^2 d\gamma(x, y) = RW_2(\mu_0, \mu_1)^2.$$

Thus if $RW_2(\mu_0, \mu_1) = 0$, we have $W_2(\mu_0, \mu_1) = 0$, and thus $\mu_0 = \mu_1$. On the other hand, if $\mu_0 = \mu_1$, by the identifiability of RMM_d , after resorting the index, we can assume $K_0 = K_1$, $\pi_0 = \pi_1$ and $\nu_0^k = \nu_1^k$ for all k . Then we can choose w as the identity matrix, which means $RW_2(\mu_0, \mu_1) \leq 0$.

Lastly, we only need to prove the triangle inequality, i.e.

$$RW_2(\mu_0, \mu_1) + RW_2(\mu_1, \mu_2) \geq RW_2(\mu_0, \mu_2)$$

for any $\mu_0, \mu_1, \mu_2 \in RMM_d$. Denote the probability vector associated with μ_0, μ_1, μ_2 by π_0, π_1, π_2 , the components of μ_j by ν_j^k and the sizes by K_0, K_1, K_2 . Let $w^{01}(w^{12})$ be the solution to (3.2) with marginals $\pi_0, \pi_1(\pi_1, \pi_2)$. Define w^{02} by

$$w_{kl}^{02} = \sum_{j=1}^{K_1} \frac{w_{kj}^{01} w_{jl}^{12}}{\pi_1^j}.$$

If $\pi_1^j = 0$, the corresponding term is set to 0. Then $w^{02} \in \Pi(\pi_0, \pi_2)$, which follows from

$$\sum_k w_{kl}^{02} = \sum_j w_{jl}^{12} = \pi_2^l, \quad \forall l = 1, 2, \dots, K_2,$$

$$\sum_l w_{kl}^{02} = \sum_j w_{kj}^{01} = \pi_0^k \quad \forall k = 1, 2, \dots, K_0.$$

Therefore,

$$\begin{aligned} RW_2(\mu_0, \mu_2) &\leq \sqrt{\sum_{k,l} w_{kl}^{02} W_2(\nu_0^k, \nu_2^l)^2} = \sqrt{\sum_{k,l,j} \frac{w_{kj}^{01} w_{jl}^{12}}{\pi_1^j} W_2(\nu_0^k, \nu_2^l)^2} \\ &\leq \sqrt{\sum_{k,l,j} \frac{w_{kj}^{01} w_{jl}^{12}}{\pi_1^j} \left[W_2(\nu_0^k, \nu_1^j) + W_2(\nu_1^j, \nu_2^l) \right]^2} \\ &\leq \sqrt{\sum_{k,l,j} \frac{w_{kj}^{01} w_{jl}^{12}}{\pi_1^j} W_2(\nu_0^k, \nu_1^j)^2} + \sqrt{\sum_{k,l,j} \frac{w_{kj}^{01} w_{jl}^{12}}{\pi_1^j} W_2(\nu_1^j, \nu_2^l)^2} \\ &= \sqrt{\sum_{k,j} w_{kj}^{01} W_2(\nu_0^k, \nu_1^j)^2} + \sqrt{\sum_{l,j} w_{jl}^{12} W_2(\nu_1^j, \nu_2^l)^2} \\ &= RW_2(\mu_0, \mu_1) + RW_2(\mu_1, \mu_2). \end{aligned}$$

In the above, the second inequality is due to the triangle inequality of W_2 , and the third inequality comes from the Minkowski inequality. \blacksquare

Note that this distance is quite easier to compute than Wasserstein distance, since we do not need to discretize the radial mixtures in space. We only need to compute the Monge transport map for two 1-dimensional distributions as discussed in subsection 2.2 and a linear programming with $K_0 \cdot K_1$ variables.

3.2. The space (RMM_d, RW_2) is a geodesic space.

Theorem 3.4. *Let $\mu_0, \mu_1 \in RMM_d$ be written as in (3.1). The displacement interpolation on (RMM_d, RW_2) connecting μ_0 and μ_1 is given by*

$$(3.4) \quad \mu_t = \sum_{k,l} w_{kl}^* \nu_t^{kl},$$

where ν_t^{kl} is the displacement interpolation between ν_0^k and ν_1^l , and

$$(3.5) \quad RW_2(\mu_s, \mu_t) = (t-s)RW_2(\mu_0, \mu_1), \quad 0 \leq s \leq t \leq 1.$$

Proof. For any $0 \leq s \leq t \leq 1$, we have

$$RW_2(\mu_s, \mu_t) \leq \sqrt{\sum_{k,l} w_{kl}^* W_2(\nu_s^{kl}, \nu_t^{kl})^2} = (t-s) \sqrt{\sum_{k,l} w_{kl}^* W_2(\nu_0^k, \nu_1^l)^2} = (t-s)RW_2(\mu_0, \mu_1).$$

The inequality is given by choosing the transport plan as transporting all mass of ν_s^{kl} to ν_t^{kl} , and the equality is given by (2.4). It follows that

$$\begin{aligned} &RW_2(\mu_0, \mu_s) + RW_2(\mu_s, \mu_t) + RW_2(\mu_t, \mu_1) \\ &\leq sRW_2(\mu_0, \mu_1) + (t-s)RW_2(\mu_0, \mu_1) + (1-t)RW_2(\mu_0, \mu_1) = RW_2(\mu_0, \mu_1). \end{aligned}$$

On the other hand, according to (3.3), we have

$$RW_2(\mu_0, \mu_s) + RW_2(\mu_s, \mu_t) + RW_2(\mu_t, \mu_1) \geq RW_2(\mu_0, \mu_1).$$

Therefore, we obtain (3.5). ■

Compared to the geodesic path defined by W_2 , the distributions on the RW_2 geodesic all keep the radial mixture structure. The examples can be seen in section 4.

3.3. The transport map defined in (RMM_d, RW_2) . In many cases, we not only need the transport plan, but also need a transport map. Let μ_0 and μ_1 be two radial mixtures. We have proved that γ defined in (3.3) is a transport plan of the two RMM marginals. Thus we have two natural ways to define the transport map. The first way is setting

$$(3.6) \quad T_{\text{mean}}(x) = \mathbb{E}_\gamma(Y|X = x),$$

where (X, Y) is distributed according to γ in (3.3). The distribution of $Y|X = x$ is given by the discrete distribution

$$(3.7) \quad \sum_{k,l} p_{k,l}(x) \delta_{T_{kl}(x)} \quad \text{with} \quad p_{k,l}(x) = \frac{\sum_{k,l} w_{k,l}^* \rho_0(x; m_0^k, c_0^k)}{\sum_j \pi_0^j \rho_0(x; m_0^k, c_0^k)}.$$

We can get that

$$(3.8) \quad T_{\text{mean}}(x) = \frac{\sum_{k,l} w_{k,l}^* \rho_0(x; m_0^k, c_0^k) T_{kl}(x)}{\sum_j \pi_0^j \rho_0(x; m_0^k, c_0^k)}.$$

This seems to be the most natural way to define a transport map. However, $(T_{\text{mean}})_\# \mu_0$ may be far from μ_1 . For instance, given three radially contoured distributions $\nu_0 = R_1(0, 1, \rho)$, $\nu_1 = R_1(a, 1, \rho)$, $\nu_2 = R_1(-a, 1, \rho)$, we define $\mu_0 = \nu_0$ and $\mu_1 = 0.5\nu_1 + 0.5\nu_2$. In this case, T_{mean} is the identity map, and thus $(T_{\text{mean}})_\# \mu_0 = \mu_0$, which will be very far from μ_1 when a is large.

Based on (3.7), another way to define a transport map is setting

$$(3.9) \quad T_{\text{rand}}(x) = T_{kl}(x) \quad \text{with probability} \quad p_{k,l}(x) = \frac{\sum_{k,l} w_{k,l}^* \rho_0(x; m_0^k, c_0^k)}{\sum_j \pi_0^j \rho_0(x; m_0^k, c_0^k)}.$$

As it has been discussed in [10], $(T_{\text{rand}})_\# \mu_0$ would be equal in expectation to μ_1 .

3.4. The comparison between RW_2 and W_2 .

Proposition 3.5 (The comparison between RW_2 and W_2). *Let $\mu_0, \mu_1 \in RMM_d$ be written as in (3.1), then*

$$(3.10) \quad W_2(\mu_0, \mu_1) \leq RW_2(\mu_0, \mu_1) \leq W_2(\mu_0, \mu_1) + \sum_{j=0,1} \left[2 \sum_{k=1}^{K_j} \pi_j^k (c_j^k)^2 \frac{\int_0^{+\infty} r^{d+1} \rho_j(r) dr}{\int_0^{+\infty} r^{d-1} \rho_j(r) dr} \right]^{\frac{1}{2}}.$$

Proof. The first inequality has already been proved in (3.3). The proof of the second inequality is similar to the proof of Proposition 6 in [10]. ■

The first inequality shows that RW_2 distance is lower bounded by W_2 distance. The second inequality shows that when given two generators, RW_2 distance is upper bounded by W_2 plus a term that only depends on the parameters $\{c_j^k\}$. Therefore, when $\max_{j,k}\{c_j^k\} \leq \varepsilon$, we have

$$RW_2(\mu_0, \mu_1) \leq W_2(\mu_0, \mu_1) + C\varepsilon,$$

where C is a constant depending on the dimension d and generators ρ_0, ρ_1 .

3.5. The barycenter in (RMM_d, RW_2) .

Definition 3.6 (RW_2 barycenter). *Let $\mu_1, \mu_2, \dots, \mu_N \in RMM_d$, where*

$$\mu_j = \sum_{k=1}^{K_j} \pi_j^k \nu_j^k, \quad \nu_j^k = R_d(m_j^k, c_j^k, \rho_j), \quad j = 1, 2, \dots, N,$$

and $\lambda = (\lambda_1, \lambda_2, \dots, \lambda_N) \in \Gamma_K$ is a weight vector. The RW_2 barycenter μ of the μ_j with weights $\{\lambda_j\}$ is a solution of

$$(3.11) \quad \inf_{\mu \in RMM_d} \sum_{j=1}^N \lambda_j RW_2(\mu_j, \mu)^2.$$

The definition of RW_2 barycenter involves a variational problem, which is difficult to handle. To get a more specific description of the RW_2 barycenter, we consider a multimarginal problem as follows:

$$(3.12) \quad MRW_2(\mu_1, \mu_2, \dots, \mu_N)^2 = \min_{w \in \Pi(\pi_1, \pi_2, \dots, \pi_N)} \sum_{k_1, \dots, k_N=1}^{K_1, \dots, K_N} w_{k_1 \dots k_N} BW_2(\nu_1^{k_1}, \dots, \nu_N^{k_N})^2,$$

where $\Pi(\pi_1, \pi_2, \dots, \pi_N)$ is the set of tensors w having $\pi_1, \pi_2, \dots, \pi_N$ as marginals, i.e.

$$\sum_{\substack{k_1, \dots, k_{j-1}, k_{j+1}, \dots, k_N \\ k_j=k}} w_{k_1 \dots k_N} = \pi_j^k, \quad \forall j \in \{1, \dots, N\}, k \in \{1, \dots, K_j\}.$$

The two problems are linked by the following theorem.

Theorem 3.7. *Let $\mu_1, \mu_2, \dots, \mu_N \in RMM_d$, then*

$$\inf_{\mu \in RMM_d} \sum_{j=1}^N \lambda_j RW_2(\mu_j, \mu)^2 = MRW_2(\mu_1, \mu_2, \dots, \mu_N)^2.$$

Let $w^* \in \Pi(\pi_1, \dots, \pi_N)$ be the solution of (3.12), and $\nu^{k_1 \dots k_N}$ be the barycenter of $\nu_1^{k_1}, \dots, \nu_N^{k_N}$ with weights $\{\lambda_j\}_{j=1}^N$. The RW_2 barycenter μ of μ_j with weights $\{\lambda_j\}_{j=1}^N$ is given by

$$\mu = \sum_{k_1 \dots k_N} w_{k_1 \dots k_N}^* \nu^{k_1 \dots k_N}.$$

Moreover, the number of components of this barycenter is no more than $K_1 + K_2 + \cdots + K_N - N + 1$.

Proof. For any $\mu \in RMM_d$, we write $\mu = \sum_{l=1}^L \pi^l \nu^l$. Let w^j be the RW_2 optimal plan between the mixtures μ_j and μ . We define a $K_1 \times \cdots \times K_N \times L$ tensor α and a $K_1 \times \cdots \times K_N$ tensor $\bar{\alpha}$ by

$$\alpha_{k_1 \cdots k_N l} = \frac{\prod_{j=1}^N w_{k_j l}^j}{(\pi^l)^N}, \quad \text{and} \quad \bar{\alpha}_{k_1 \cdots k_N} = \sum_{l=1}^L \alpha_{k_1 \cdots k_N l}.$$

Clearly $\alpha \in \Pi(\pi_1, \cdots, \pi_N, \pi)$ and $\bar{\alpha} \in \Pi(\pi_1, \cdots, \pi_N)$. Moreover,

$$\begin{aligned} \sum_{j=1}^N \lambda_j RW_2(\mu_j, \mu)^2 &= \sum_{j=1}^N \lambda_j \sum_{k_j=1}^{K_j} \sum_{l=1}^L w_{k_j l}^j W_2(\nu_j^{k_j}, \nu^l)^2 \\ &= \sum_{j=1}^N \lambda_j \sum_{k_1 \cdots k_N, l} \alpha_{k_1 \cdots k_N l} W_2(\nu_j^{k_j}, \nu^l)^2 = \sum_{k_1 \cdots k_N, l} \alpha_{k_1 \cdots k_N l} \sum_{j=1}^N \lambda_j W_2(\nu_j^{k_j}, \nu^l)^2 \\ &\geq \sum_{k_1 \cdots k_N, l} \alpha_{k_1 \cdots k_N l} BW_2(\nu_1^{k_1}, \dots, \nu_N^{k_N})^2 = \sum_{k_1 \cdots k_N} \bar{\alpha}_{k_1 \cdots k_N} BW_2(\nu_1^{k_1}, \dots, \nu_N^{k_N})^2 \\ &\geq MRW_2(\mu_1, \dots, \mu_N)^2. \end{aligned}$$

This inequality holds for all $\mu \in RMM_d$. Thus

$$\inf_{\mu \in RMM_d} \sum_{j=1}^N \lambda_j RW_2(\mu_j, \mu)^2 \geq MRW_2(\mu_1, \mu_2, \dots, \mu_N)^2.$$

Conversely, let $w^* \in \Pi(\pi_1, \cdots, \pi_N)$ be the solution of (3.12) and $\nu^{k_1 \cdots k_N}$ be the barycenter of $\nu_1^{k_1}, \dots, \nu_N^{k_N}$ with weights $\{\lambda_j\}_{j=1}^N$. We define $\mu = \sum_{k_1 \cdots k_N} w_{k_1 \cdots k_N}^* \nu^{k_1 \cdots k_N}$. Based on the results in subsection 2.2, $\nu^{k_1 \cdots k_N}$ is still a radially contoured distribution, and thus $\mu \in RMM_d$. We define RW_2 plans $\{w^j\}_{j=1}^N$ between $\{\mu_j\}_{j=1}^N$ and μ by

$$w_{i_j, k_1 \cdots k_N}^j = \begin{cases} w_{k_1 \cdots k_N}^*, & i_j = k_j, \\ 0, & i_j \neq k_j, \end{cases}$$

where $1 \leq i_j \leq K_j$. It is clearly $w^j \in \Pi(\pi_j, w)$. Then we have

$$\begin{aligned}
MRW_2(\mu_1, \mu_2, \dots, \mu_N)^2 &= \sum_{k_1 \dots k_N} w_{k_1 \dots k_N}^* BW_2(\nu_1^{k_1}, \dots, \nu_N^{k_N})^2 \\
&= \sum_{k_1 \dots k_N} w_{k_1 \dots k_N}^* \sum_{j=1}^N \lambda_j W_2(\nu_j^{k_j}, \nu^{k_1 \dots k_N})^2 = \sum_{j=1}^N \lambda_j \sum_{k_1 \dots k_N} w_{k_1 \dots k_N}^* W_2(\nu_j^{k_j}, \nu^{k_1 \dots k_N})^2 \\
&= \sum_{j=1}^N \lambda_j \sum_{i_j} \sum_{k_1 \dots k_N} w_{i_j, k_1 \dots k_N}^j W_2(\nu_j^{i_j}, \nu^{k_1 \dots k_N})^2 \geq \sum_{j=1}^N \lambda_j RW_2(\mu_j, \mu)^2 \\
&\geq 0 \inf_{\mu \in RMM_d} \sum_{j=1}^N \lambda_j RW_2(\mu_j, \mu)^2.
\end{aligned}$$

Therefore,

$$\inf_{\mu \in RMM_d} \sum_{j=1}^N \lambda_j RW_2(\mu_j, \mu)^2 = MRW_2(\mu_1, \mu_2, \dots, \mu_N)^2.$$

Moreover, since $MRW_2(\mu_1, \mu_2, \dots, \mu_N)^2 \geq \sum_{j=1}^N \lambda_j RW_2(\mu_j, \mu)^2$, we get that μ is a RW_2 barycenter of μ_j with weights $\{\lambda_j\}_{j=1}^N$. Since (3.12) is a linear program with $K_1 + \dots + K_N - N + 1$ linear constraints, the solution w^* can not have more than $K_1 + \dots + K_N - N + 1$ nonzero elements. Therefore, the barycenter has more than $K_1 + \dots + K_N - N + 1$ components. \blacksquare

Theorem 3.7 shows that the RW_2 barycenter is a combination of the Wasserstein barycenters of the components, and the functional optimal problem (3.11) can be reduced to a linear programming problem. Therefore, to compute an RW_2 barycenter, we only need to compute the Wasserstein barycenters of radial components of the marginals and solve a linear programming problem. When the marginals come from the same family $RMM_d(\rho)$, their RW_2 barycenter can be easily computed since the Wasserstein barycenter of radially contoured distributions $\{\mu_j = R_d(m_j, c_j, \rho)\}_{j=1}^N$ with weights $\{\lambda_j\}_{j=1}^N$ is simply $R_d(m_*, c_*, \rho)$, where $m_* = \sum_{j=1}^N \lambda_j m_j$ and $c_* = \sum_{j=1}^N \lambda_j c_j$. In this case, only a linear programming problem need to be solved, and thus the RW_2 barycenter is quite easier to compute than Wasserstein barycenter. In addition, the Wasserstein barycenter of radial mixtures is usually not a radial mixtures. However, our RW_2 will keep this structure.

3.6. Some remarks on our method. In the framework given in [10], the mixtures are identifiable and the components satisfy marginal consistency, where the marginal consistency requirement is important in the GW_2 definition. Their definition of GW_2 between two d -dimensional mixtures from the same family restricts the transport plan to the space of $2d$ -dimensional mixtures. However, our RW_2 is not defined in that way. In our framework, only the identifiability is required. To show the importance of identifiability of $RMM_d(\rho)$, we consider the following instance. Let $\rho_U(x) = \mathbb{1}_{[0,1]}(x)$ be the indicator function on $[0, 1)$ and let μ_0 be the uniform distribution on $(-1, 1)$, which can be written as $R_1(0, 1, \rho)$. Define

$\nu^0 = R_1(0, 2, \rho_U)$, $\nu^1 = R_1(1, 2, \rho_U)$, and

$$d\mu_1(x) = 0.5d\nu^0(x) + 0.5d\nu^1(x).$$

We then have $\mu_1 \in RMM_1(\rho_U)$ and $\mu_0 = \mu_1$, which means that the mixtures in $RMM_1(\rho_U)$ are not identifiable. However, by the definition of RW_2 in (3.2), w^* can only be chosen as $(0.5, 0.5)$, which follows that

$$RW_2(\mu_0, \mu_1) = \sqrt{0.5W_2(\mu_0, \nu^0)^2 + 0.5W_2(\mu_0, \nu^1)^2} > 0,$$

and thus RW_2 is not a distance on $RMM_1(\rho_U)$.

Another question is whether we can generalize RW_2 from the radially contoured case to the general elliptically contoured case. An elliptically contoured distribution on \mathbb{R}^d has a density of the form

$$f_{m, \Sigma}(x) = \frac{1}{Z} \rho \left((x - m)^\top \Sigma^{-1} (x - m) \right), \quad \forall x \in \mathbb{R}^d,$$

where Z is the normalizer, $m \in \mathbb{R}^d$, Σ is a positive definite matrix of size $d \times d$, and ρ is a positive generator defined on \mathbb{R}_+ . We denote the set of all identifiable finite mixtures of elliptically contoured distributions with generator ρ as $EMM_d(\rho)$ and the union of such $EMM_d(\rho)$ as EMM_d . For example, when choosing $\rho(x) = \exp(-x)$, $EMM_d(\rho) = GMM_d$. The generalization to $EMM_d(\rho)$ is almost trivial thanks to the results in [16, 18, 1]. [16] and [18] give the distance and the Monge map of two elements in $EMM_d(\rho)$, and after a little modification of the proof of Theorem 6.1 in [1], one can show that the barycenter of elements in $EMM_d(\rho)$ is still in $EMM_d(\rho)$. With these properties, we can easily generalize our results to $EMM_d(\rho)$. While [10] has a similar generalization, the generalization in our way does not require the marginal consistency. However, our results can not be further generalized to EMM_d . In [8], it is shown that the barycenter of two elliptically contoured distributions need not to be elliptically contoured. Since the RW_2 barycenters are mixtures of barycenters of the elliptically contoured components of the marginal mixtures, their components need not to be elliptically contoured. In other words, the RW_2 barycenter of two elements in EMM_d can not belong to EMM_d .

4. Some examples for radial mixtures. In this section, we compare RW_2 barycenters with W_2 barycenters using two kinds of generators in 1-dimensional and 2-dimensional cases. In each case, we fix the generator ρ and compute the W_2 barycenters and RW_2 barycenters of given distributions in $RMM_d(\rho)$. The W_2 barycenters are all computed using Sinkhorn algorithm with regularization parameter 5×10^{-4} in 1-dimensional case and 5×10^{-3} in 2-dimensional case. The 1-dimensional case is computed on a grid containing 100 points, and the 2-dimensional case is computed on a grid containing 50 points per dimension.

In terms of the computation cost, it is difficult to find a standard to compare the two methods. The computation cost of W_2 barycenters highly depends on the choice of the grid and the regularization parameter, but the computation cost of RW_2 barycenters only depends on the number of parameters of radial mixtures. In our setting, the order of magnitude of an RW_2 barycenter is 2 ms while that of a 1-dimensional W_2 barycenter is 30 ms and that

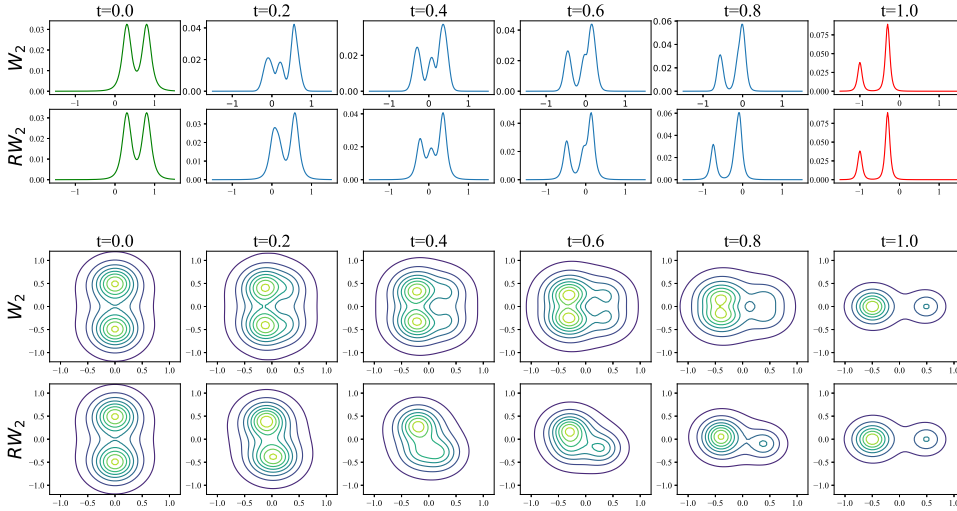


Figure 1. 1-d and 2-d examples for RW_2 and W_2 barycenters of two mixtures of radially contoured distributions with generator ρ_{IMQ} . In each case, the first row is the W_2 interpolation and the second row is the RW_2 interpolation.

of a 2-dimensional W_2 barycenter is 3 s. Therefore, compared to the computation of RW_2 barycenters, the computation of W_2 is more expensive in several orders of magnitude.

4.1. Radial mixtures based on inverse multi-quadratic functions. The multi-quadratic function $(1 + x^2)^\alpha$ plays an important role in RBF theory. To ensure such function can be used as a generator, we need α to be negative. That is the inverse multi-quadratic (IMQ) function

$$(4.1) \quad \rho_{IMQ}(x) = (1 + x^2)^{-\beta}, \quad \beta > 0.$$

To ensure the corresponding distribution is in $\mathcal{P}_2(\mathbb{R}^d)$, it requires that $\beta > d/2$. The radially contoured distribution with generator ρ_{IMQ} is a special d -dimensional t -distribution with a scalar covariance matrix. The identifiability of finite mixtures of such distributions has been proved in Example 1 of [20]. Here we provide 1-dimensional and 2-dimensional cases of W_2 and RW_2 barycenters for mixtures of such radially contoured distributions in Figure 1. In each case, we set $\beta = 2$ and plot the interpolations induced by Wasserstein distance W_2 and RW_2 .

We observe that the behaviors of the two types of barycenters are quite different. In 1-d case, the third peak appears later in RW_2 barycenters than that appears in W_2 barycenters. In 2-d case, the W_2 barycenters are all symmetric about the x axis, while the RW_2 barycenters seem like a scaling and rotation of the components.

4.2. Radial mixtures based on compactly supported functions. The compactly supported function is another important class of basis functions in RBF theory. The simplest one is the hat function $\rho_H(x) = \max\{1 - x, 0\}$. However, the finite mixture of radially contoured

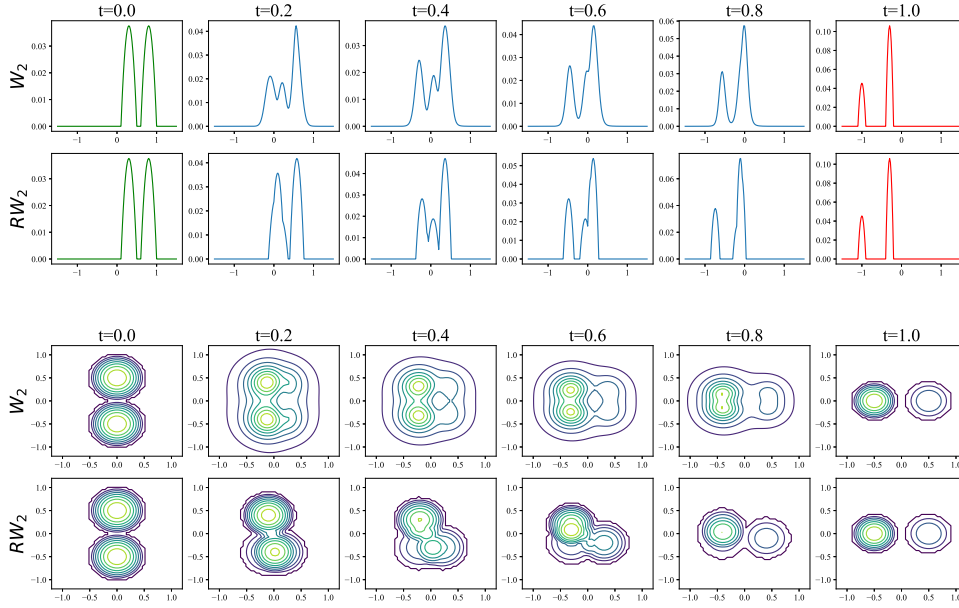


Figure 2. 1-d and 2-d examples for RW_2 and W_2 barycenters of two mixtures of radially contoured distributions with generator ρ_C . In each case, the first row is the W_2 interpolation and the second row is the RW_2 interpolation.

distributions with such generator is not identifiable. It can be found in Example 6 in [20]. Here we consider the distributions based on such compactly supported function

$$(4.2) \quad \rho_C(x) = \begin{cases} (1-x^2)^{\frac{1}{\beta}}, & 0 \leq x \leq 1, \\ 0, & x > 1, \end{cases} \quad \beta > 0.$$

The identifiability of finite mixtures of such distributions can be easily proved in ways similar to Theorem 3 in [20]. We also give the corresponding examples of 1-dimensional and 2-dimensional case in Figure 2. We set $\beta = 2$ in 1-dimensional case and $\beta = 3$ in 2-dimensional case and plot the interpolations induced by Wasserstein distance W_2 and our RW_2 .

The densities of the two marginals are not smooth on the boundaries of their supports due to the rectangular grid. We observe that the densities of RW_2 barycenters keep nonsmooth on the boundary, but those of the W_2 barycenters do not due to the regularization of Sinkhorn algorithm. Other behaviors are similar to the results presented in the previous section.

5. Using radial mixtures in practice.

5.1. Approximating discrete distributions with radial mixture models. An efficient method to approximate discrete distributions by mixture models is using EM algorithm. However, without the explicit formulation as in GMM estimation, there remains an optimization problem in each iteration of the RMM estimation, which makes the computation much slower.

To speed up this process, we introduce mini-batch and stochastic technique. The algorithm is illustrated in Algorithm 5.1.

Algorithm 5.1 mini-batch stochastic EM for RMM

Require: dataset $X = \{x_1, x_2, \dots, x_N\}$, initial parameters $\pi^0 = \{\pi_1^0, \pi_2^0, \dots, \pi_K^0\}$, $m^0 = \{m_1^0, m_2^0, \dots, m_K^0\}$, $c^0 = \{c_1^0, c_2^0, \dots, c_K^0\}$, batch size N_0 .

- 1: **while** not converged **do**
 - 2: Randomly choose N_0 points $\{\bar{x}_1, \bar{x}_2, \dots, \bar{x}_{N_0}\}$ from X ;
 - 3: **for** $(i, k) \in \{1, 2, \dots, N_0\} \times \{1, 2, \dots, K\}$ **do**
 - 4: $\tau_{ik} = \frac{\pi_k^t \rho(\bar{x}_i; m_k^t, c_k^t)}{\sum_{k=1}^K \pi_k^t \rho(\bar{x}_i; m_k^t, c_k^t)}$;
 - 5: **end for**
 - 6: $Q(m, c) = \sum_{i=1}^{N_0} \sum_{k=1}^K \tau_{ik} \log(\pi_k^t \rho(\bar{x}_i; m_k, c_k))$;
 - 7: **for** $k \in \{1, 2, \dots, K\}$ **do**
 - 8: $\pi_k^{t+1} = \sum_{i=1}^{N_0} \tau_{ik}$
 - 9: **end for**
 - 10: $m^{t+1}, c^{t+1} = \operatorname{argmax}_{m, c} Q(m, c)$;
 - 11: $t = t + 1$;
 - 12: **end while**
 - 13: **return** π^t, m^t, c^t .
-

Such technique is useful in optimization for large scaling problems [6, 29]. In the experiments shown in subsection 5.2, we use Algorithm 5.1 with initialized π^0, m^0, c^0 from K-means algorithm, a batch size 100 and a maximum number of iterations 1500. The order of magnitude for getting the parameters is several minutes, which is acceptable in practice. After getting the densities of the radial mixtures, we can use T_{mean} or T_{rand} to replace the position of Monge map in application.

5.2. Application in color transfer and color averaging. We apply our method to the color transfer problem. The color transfer problem requires a source image and a target image. We need to transfer the color style of the source image to that of the target image, so that the output image has the same pattern and geometry as the source image but with the color palette from the target image. Mathematically, an image of size $n_r \times n_c$ can be viewed as a map $u : \Omega \rightarrow \mathbb{R}^3$, where $\Omega = \{0, 1, \dots, n_r - 1\} \times \{0, 1, \dots, n_c - 1\}$. For each pixel $i \in \Omega$, $u(i) = (r_i, g_i, b_i)$ represents the color of pixel i in RGB space, where the elements r_i, g_i and b_i correspond to the intensities of red, green and blue. In color transfer task, given two images u_0 and u_1 on grids Ω_0 and Ω_1 , define the discrete color distributions of the two images as $\eta_k = \frac{1}{|\Omega_k|} \sum_{i \in \Omega_k} \delta_{u_k(i)}$, $k = 0, 1$. We need to find a color transfer map $T : \mathbb{R}^3 \rightarrow \mathbb{R}^3$ which makes $T_{\#} \eta_0$ close to η_1 . To utilize our framework, we first approximate the two discrete distributions with two radial mixtures and then compute the transport map. Although our method allows the radial mixtures to come from different families, it will be necessary to solve for the function T in (2.7) by numerical method in this case, which significantly increases the computation complexity. Therefore, in our experiments, we always use radial mixtures with the same generator. In this experiment, the source image u_0 of size 432×576 and the target image u_1 of size 360×480 are shown in Figure 3.



Figure 3. Left, the source image u_0 . Right, the target image u_1 .

We will compare our method with that based on GMM proposed in [10]. The generator we choose is the inverse multi-quadratic function ρ_{IMQ} given in subsection 4.1 with $\beta = 3$. The corresponding RMM here we will call IMQ-MM. In both methods, we first use the mixture models to approximate the color distributions of the two images and then compute T_{mean} as the transport map, since T_{rand} will give a noisier result which has been shown in [10]. Because T_{mean} is not a measure preserving map as discussed in subsection 3.3, the first thing we care is how far it is between T_{mean} and a transport map. We use the following value as a principle:

$$(5.1) \quad \text{error} = W_2((T_{\text{mean}})_{\#}\eta_0, \eta_1)^2.$$

If T_{mean} is a transport map, we have $(T_{\text{mean}})_{\#}\eta_0 = \eta_1$, and the error will be 0. Intuitively, while increasing the number of components, approximation will be better. We plot error vs the number of components on the left of Figure 4. On the other hand, a typical advantage of RMM over GMM is that when we fix the number of components, n , GMM needs to fit one weight vector, n mean vectors, and n covariance matrices, which correspond to $(1 + 1.5d + 0.5d^2)n$ parameters, where d is the dimension of the underlying space, but RMM only needs to fit $(d + 2)n$ parameters. The color transfer task is a 3-dimensional problem. Thus the number of parameters in GMM is $10n$, whereas that in RMM is $5n$. We also plot the error vs the number of parameters on the right of Figure 4. Here the color distributions of the images are all approximated by mixture models with the same number of components. Note that the OT problem (5.1) is too large to compute. Thus, in this experiment, we randomly choose m pixels in each image as η_0^m and η_1^m and compute the W_2 distance between $(T_{\text{mean}})_{\#}\eta_0^m$ and η_1^m . Here we set $m = 5000$ and repeat the process 50 times. Each error value shown in Figure 4 is the average of the results computed 10 times. The theoretical fundamental of this operation is based on the results of [12], which reads

$$E \left(\left| W_2(\hat{\alpha}_n, \hat{\beta}_n) - W_2(\alpha, \beta) \right| \right) = O \left(n^{-\frac{1}{d}} \right),$$

where $\hat{\alpha}_n$ and $\hat{\beta}_n$ are discrete distributions of n samples from compactly supported probability

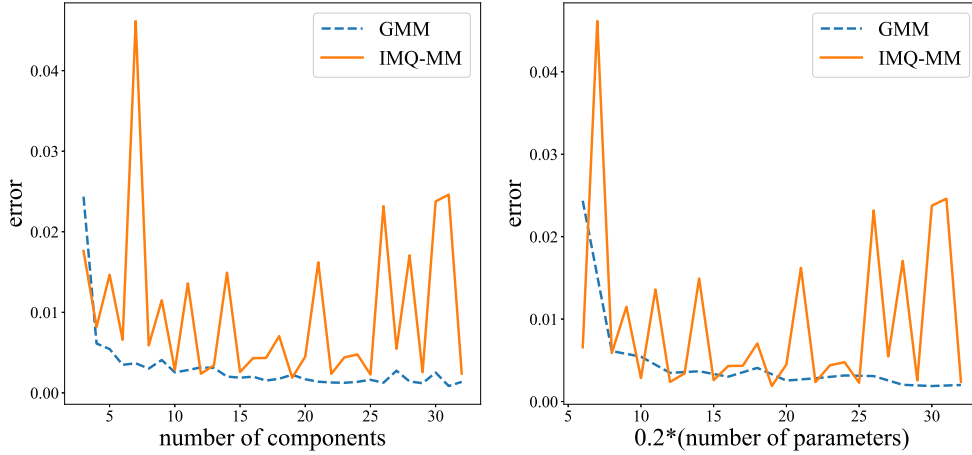


Figure 4. The relationship between error (The square of W_2 distance between the distributions of transferred source palette and the target palette) and the number of components(left) and the number of parameters(right). We find that the results of GMM is stable than that of IMQ-MM. When we compare the performance under the same number of components, GMM performs better in most of the time. However, when constrained to the identical number of parameters, the two methods demonstrate comparable results.

distributions α and β .

Figure 4 shows that the error of GMM is more stable than that of IMQ-MM. It can be attributed to the elliptical shape of GMM components, which enables superior adaptability to practical data distribution, whereas the radial configuration of the components of IMQ-MM renders its fitting performance more sensitive to the number of components. In the left figure, better performance of GMM over IMQ-MM in most scenarios is partially attributable to its utilization of twice as many parameters as in IMQ-MM. When constrained to an identical parameter count, the two models show comparable performance, as is revealed in the right figure. Furthermore, our results indicate that the increasing of the number of components does not significantly reduce the error, but increases the computation complexity. After a trade-off between the error performance and computational efficiency, we choose 10 components for GMM and 15 components for IMQ-MM. The results are shown in the first row of Figure 5.

We find that the image transferred by IMQ-MM is lighter than by GMM. Both images successfully keep the pattern and geometry of the source image. We further consider the differences of the color distributions between the target image and the two transferred images. We plot the projections of these color distributions on RGB space to B&R space and G&R space in the last two rows in Figure 5. It is clear that GMM gives a “thinner” distribution than the target distribution. Especially in the G&R space, some points of the target distribution are lost. However, the distribution given by IMQ-MM is “fatter” than the target distribution. Both results have some differences from the target distribution, but IMQ-MM seems better in this experiment.

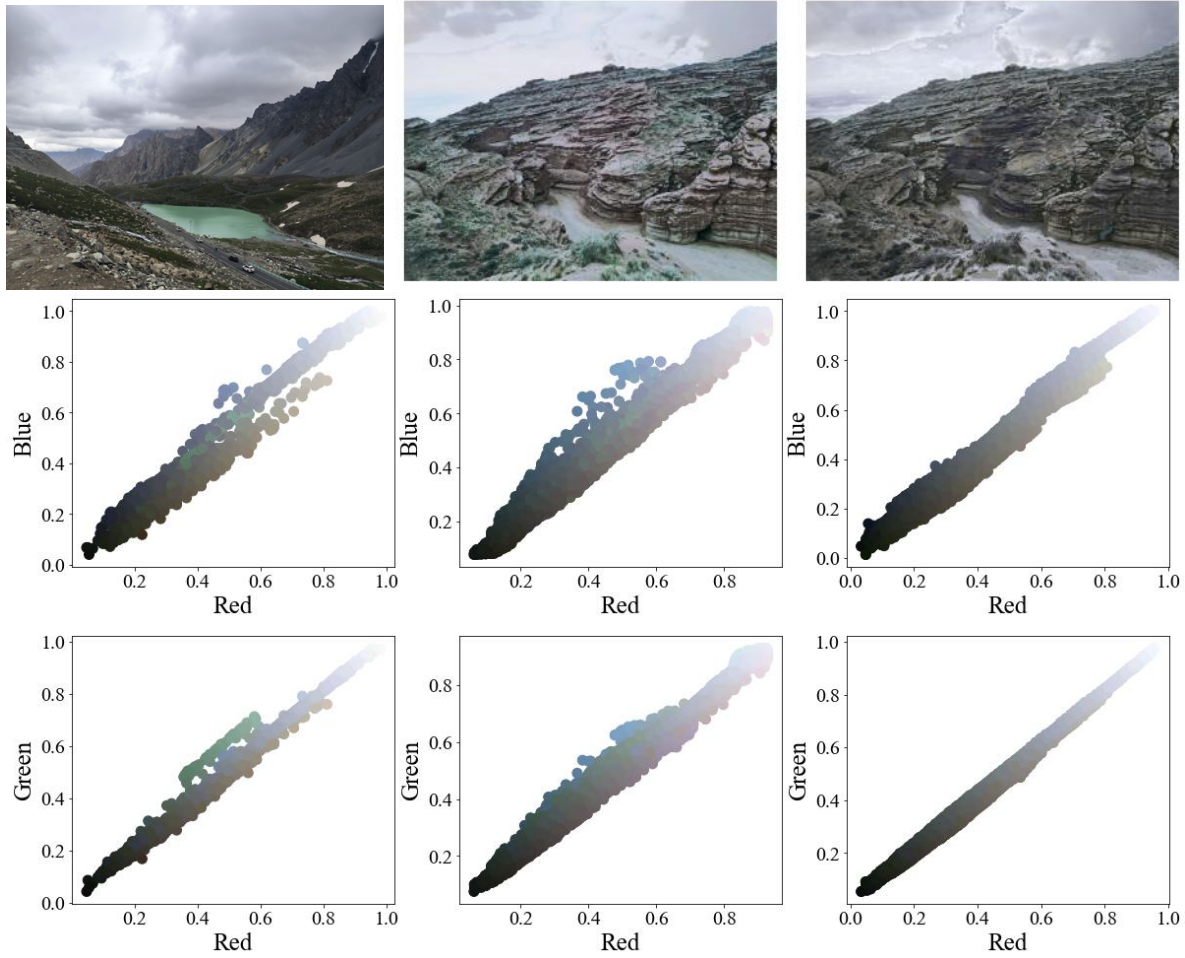


Figure 5. First row: left, the target image. Middle, the transferred image by IMQ-MM. Right, the transferred image by GMM. Second row, the projections of color palettes of images to blue and red space. Left, the target image. Middle, the top left image. Right, the top right image. Third row, the projections of color palettes of images to red and green space. The order is the same.

In terms of the cost of computation, our method based on IMQ function is slower than GMM. The order of magnitude for outputting the top middle image in Figure 5 is 5 minutes and that for outputting the top right image is 50 seconds. The main cost is spent in the EM algorithm in this experiment. When we use EM algorithm to update the parameters, there exists an explicit formulation in each step of GMM. However, each updating step in IMQ-MM requires us to solve an optimization problem.

We end this section with a color averaging experiment showed in Figure 6. Three images are given at the top. The color palettes of the images are represented by RMMs with 14 components each. We show the images transferring the color palette of the top middle image to the RW_2 barycenters of the 3 color palettes. The barycenter weight of the bottom left



Figure 6. In this experiment, the top middle image is modified in such way that its color distribution goes through the $IMQ-W_2$ barycenters of the color distributions of the top 3 images. Each source is approximated by an IMQ -mixture of 14 components. The weights used in the barycenters are the barycenter coordinates with respect to the top 3 images of the top 3 images in the triangle. The weight of the bottom left one is 1 of the top left image and that of the bottom right one is 1 of the top right image.

corner is 1 of the top left image and that of the bottom right one is 1 of the top right image. The weights of other images are the corresponding barycenter coordinates. For example, the weight of the second image in the third line is $(1/3, 1/3, 1/3)$.

6. Conclusions and remarks. In this paper, we define a relaxed Wasserstein distance RW_2 on the set of all identifiable RMMs by viewing the RMMs as discrete distributions in the space of radially contoured distributions. We show that RMM_d equipped with RW_2 is a geodesic space, and the computation of transport plan and barycenter in this space is quite easier than in Wasserstein space. Compared to GW_2 defined in [10], which can only be generalized to $EMM_d(\rho)$ whose components satisfy marginal consistency, our RW_2 can be generalized to all the $EMM_d(\rho)$. In application, we use EM algorithm to estimate the mixtures from discrete data. Since the M-step of the EM algorithm for RMMs requires us to solve an optimization

problem while that for GMMs has an explicit formulation, the EM algorithm for RMMs is much slower than that for GMMs. In subsection 5.1, we introduce the mini-bath stochastic EM Algorithm 5.1 to speed up estimating RMMs. In an experiment of color transfer task, we have compared our method with that proposed in [10]. In this task, two methods provide comparable numerical results, and the color distribution of the output image is more desirable by our method.

This work can be extended in several ways in the future. On the one hand, for example, a relaxed Gromov-Wasserstein distance analogous to RW_2 can be developed. On the other hand, if we allow the coefficients to be negative, a continuous way to transfer a function to another can be established by fitting each function with RBFs and continuously changing the parameters.

Acknowledgments. We would like to thank Songyan Luo for the helpful discussion.

REFERENCES

- [1] M. AGUEH AND G. CARLIER, *Barycenters in the Wasserstein space*, SIAM Journal on Mathematical Analysis, 43 (2011), pp. 904–924.
- [2] J. ALTSCHULER, J. WEED, AND P. RIGOLLET, *Near-linear time approximation algorithms for optimal transport via sinkhorn iteration*, in Advances in Neural Information Processing Systems, vol. 2017-, 2017, pp. 1965–1975.
- [3] M. BAUER, S. JOSHI, AND K. MODIN, *Diffeomorphic density matching by optimal information transport*, SIAM Journal on Imaging Sciences, 8 (2015), pp. 1718–1751.
- [4] E. BOISSARD, *Simple bounds for convergence of empirical and occupation measures in 1- wasserstein distance*, Electronic Journal of Probability, 16 (2011), pp. 2296–2333.
- [5] F. BOLLEY, A. GUILLIN, AND C. VILLANI, *Quantitative concentration inequalities for empirical measures on non-compact spaces*, Probability theory and related fields, 137 (2007), pp. 541–593.
- [6] L. BOTTOU, F. E. CURTIS, AND J. NOCEDAL, *Optimization methods for large-scale machine learning*, SIAM eview, 60 (2018), pp. 223–311.
- [7] S. P. BOYD, *Convex optimization*, Cambridge University Press, Cambridge, UK ; New York, 2004.
- [8] K. CHEN AND Y. ZHANG, *Optimal Transport and Wasserstein Barycenter for Radial contoured distributions*, 2024, <https://arxiv.org/abs/2404.08383>.
- [9] M. CUTURI, *Sinkhorn distances: lightspeed computation of optimal transport*, in Proceedings of the 27th International Conference on Neural Information Processing Systems - Volume 2, NIPS’13, Red Hook, NY, USA, 2013, Curran Associates Inc., p. 2292–2300.
- [10] J. DELON AND A. DESOLNEUX, *A Wasserstein-Type Distance in the Space of Gaussian Mixture Models*, SIAM Journal on Imaging Sciences, 13 (2020), pp. 936–970.
- [11] A. P. DEMPSTER, N. M. LAIRD, AND D. B. RUBIN, *Maximum likelihood from incomplete data via the em algorithm*, Journal of the Royal Statistical Society. Series B, Methodological, 39 (1977), pp. 1–38.
- [12] R. M. DUDLEY, *The Speed of Mean Glivenko-Cantelli Convergence*, The Annals of mathematical statistics, 40 (1969), pp. 40–50.
- [13] P. DVURECHENSKY, A. GASNIKOV, AND A. KROSHNIN, *Computational optimal transport: Complexity by accelerated gradient descent is better than by sinkhorn’s algorithm*, in 35th International Conference on Machine Learning, ICML 2018, vol. 3, 2018, pp. 2196–2220.
- [14] L. EVANS, W. GANGBO, AND L. C. EVANS, *Differential Equations Methods for the Monge-Kantorovich Mass Transfer Problem*, vol. 137, American Mathematical Society, Providence, 1999.
- [15] B. GALERNE, A. LECLAIRE, AND J. RABIN, *Semi-discrete Optimal Transport in Patch Space for Enriching Gaussian Textures*, in GSI, vol. 10589, Cham, 2017, Springer International Publishing, pp. 100–108.
- [16] M. GELBRICH, *On a Formula for the L^2 Wasserstein Metric between Measures on Euclidean and Hilbert Spaces*, Mathematische Nachrichten, 147 (1990), pp. 185–203.
- [17] W. GUO, N. HO, AND M. I. JORDAN, *Fast algorithms for computational optimal transport and wasserstein*

- barycenter*, in Proceedings of Machine Learning Research, vol. 108, 2020, pp. 2088–2097.
- [18] E. GÓMEZ, M. A. GÓMEZ-VILLEGAS, AND J. M. MARÍN, *A Survey on Continuous Elliptical Vector Distributions*, Revista Matemática Complutense, 16 (2003), pp. 345–361.
- [19] T. HASTIE, R. TIBSHIRANI, AND J. FRIEDMAN, *Elements of Statistical Learning: Data Mining, Inference, and Prediction*, Springer Series in Statistics, Springer, New York, second edition ed., 2009.
- [20] H. HOLZMANN, A. MUNK, AND T. GNEITING, *Identifiability of finite mixtures of elliptical distributions*, Scandinavian journal of statistics, 33 (2006), pp. 753–763.
- [21] L. KANTOROVICH, *On the Translocation of Masses*, Journal of Mathematical Sciences (New York, N.Y.), 133 (2006), pp. 1381–1382.
- [22] J. KARLSSON AND A. RINGH, *Generalized sinkhorn iterations for regularizing inverse problems using optimal mass transport*, SIAM Journal on Imaging Sciences, 10 (2017), pp. 1935–1962.
- [23] A. KOROTIN, D. SELIKHANOVYCH, AND E. BURNAEV, *Neural Optimal Transport*, 2023, <https://arxiv.org/abs/2201.12220>.
- [24] W. A. LIGHT, *Some Aspects of Radial Basis Function Approximation*, Springer Netherlands, Dordrecht, 1992, pp. 163–190.
- [25] T. LIN, N. HO, AND M. I. JORDAN, *On efficient optimal transport: An analysis of greedy and accelerated mirror descent algorithms*, in 36th International Conference on Machine Learning, ICML 2019, vol. 2019-, 2019, pp. 7024–7033.
- [26] R. J. MCCANN, *A Convexity Principle for Interacting Gases*, Advances in Mathematics (New York, 1965), 128 (1997), pp. 153–179.
- [27] G. MONGE, *Mémoire sur la théorie des déblais et des remblais*, De l’Imprimerie Royale, Paris, 1781.
- [28] M. MUELLER, P. KARASEV, I. KOLESOV, AND A. TANNENBAUM, *Optical Flow Estimation for Flame Detection in Videos*, IEEE Transactions on Image Processing, 22 (2013), pp. 2786–2797.
- [29] A. NEMIROVSKI, A. JUDITSKY, G. LAN, AND A. SHAPIRO, *Robust stochastic approximation approach to stochastic programming*, SIAM journal on optimization, 19 (2009), pp. 1574–1609.
- [30] A. M. TEODORO, M. S. ALMEIDA, AND M. A. FIGUEIREDO, *Single-frame image denoising and inpainting using gaussian mixtures*, in ICPRAM 2015 - 4th International Conference on Pattern Recognition Applications and Methods, Proceedings, vol. 2, 2015, pp. 283–288.
- [31] J. WEED AND F. BACH, *Sharp asymptotic and finite-sample rates of convergence of empirical measures in wasserstein distance*, Bernoulli : official journal of the Bernoulli Society for Mathematical Statistics and Probability, 25 (2019), pp. 2620–2648.
- [32] Z.-M. WU AND R. SCHABACK, *Local Error Estimates for Radial Basis Function Interpolation of Scattered Data*, IMA Journal of Numerical Analysis, 13 (1993), pp. 13–27.
- [33] G. YU, G. SAPIRO, AND S. MALLAT, *Solving inverse problems with piecewise linear estimators: From gaussian mixture models to structured sparsity*, IEEE transactions on image processing, 21 (2012), pp. 2481–2499.
- [34] Y. ZHANG, *Reconstruct Multiscale Functions Using Different RBFs in Different Subdomains*, Applied Mathematics and Computation, 189 (2007), pp. 893–901.
- [35] D. ZORAN AND Y. WEISS, *From learning models of natural image patches to whole image restoration*, in IEEE, 2011, pp. 479–486.